







A Magnetic Catheter With Force Sensing Capability Toward Interventional Surgery

Xinliang Wang , Graduate Student Member, IEEE, Weida Kang , Xudong Liang , Kiwon Ban ,
Jun Liu , Senior Member, IEEE, and Jiachen Zhang , Member, IEEE

Abstract—Magnetically actuated medical instruments could greatly facilitate minimally invasive surgery (MIS). For example, onboard magnetic materials help catheters travel across tortuous lumens and reach difficult-to-access sites inside human bodies, guided by a controlled magnetic field (MF). However, permanent magnets inside the human body could cause mechanical hazards when controlled in attraction mode with a small actuation distance. Moreover, current magnetic catheters lose some dexterity when the MF source is spatially hindered by surgical facilities or the patient's body. We propose a magnetically guided catheter tipped with a solenoid and a soft force sensor. The catheter's bending direction and angle could be controlled conveniently via reversing the current direction and tuning the strength of the current, respectively. The thermal safety and operation safety in attraction mode is demonstrated in experiments. Passing through a bifurcation model and an aortic arch phantom proves its superiority in navigating efficiency and demonstrates its agility in 3D compact space. Additionally, the magnetic catheter exerts desired forces at predetermined sites and guides the laser beam spot along stable paths on the heart chamber phantom's interior wall, showing great potential in radiofrequency ablation (RFA).

Index Terms—Steerable catheters/needles, medical robots and systems, solenoid tipped catheter, magnetic navigation, soft robot applications.

I. INTRODUCTION

IN RECENT decades, MIS has become a popular choice among surgical treatments. Compared with traditional surgeries, MIS minimizes trauma, reduces hospital time, and leads to a rapid postoperative recovery. In the field of interventional

surgeries, soft continuum robots are capable of passing through tortuous and confined lumens inside the human body from a tiny insertion [1], [2]. Thus, they are endowed with great promise to conduct MIS, such as using a robotic catheter or guidewire to deal with cardiovascular and cerebrovascular diseases [3]. However, existing catheters driven by cables, tendons, and backbones [4], [5] are so bulky that they cannot enter narrow space. What's more, manual operation brings down the accuracy and consumes a lot of surgical time. Newly proposed magnetic catheters aim to address these challenges.

Magnetic catheters consist of onboard magnetic materials and could be manipulated remotely and precisely by the MF [6], instead of being manually controlled through the catheter's proximal handle beside the patient's bed. Magnetic catheters often utilize commercial Neodymium Iron Boron (NdFeB) permanent magnets, which create outstanding strength of magnetic flux density with a minimal volume. Initially, a single [7], [8] or multiple NdFeB magnets [9], [10], [11] were installed at the distal end of catheters for wireless steering. To attain various deformation modalities, NdFeB magnets were embedded in the catheter's tip with an intraoperatively programmed magnetic moment, enhancing the dexterity to avoid collision with sensitive surroundings [12]. Magnetic particles have been adopted in magnetic catheters to further downscale their dimensions. Specifically, NdFeB particles were dispersed evenly into silicone elastomers and then coated on a wire [13], or directly cast into a customized mold followed for particular magnetization profile [14], [15], [16].

However, introducing permanent magnetic materials inside human bodies may create mechanical hazards to soft tissues. Manipulating the magnetic catheter in attraction mode tends to move it closer to the strongest magnetic poles for larger deflection. However, such a positive feedback control could cause that the magnetic catheter goes out of control and crushes into the lumen walls. The accidental MF perturbation or position error of external magnets increases this sort of risks [17], [18]. Additionally, the realignment of the MF could be blocked by the human tissues or surrounding medical facilities. The permanent magnet cannot approach the targeted sites as desired, leading to insufficient magnetic flux density for navigation and even loss of actuation ability [19].

To address the aforementioned problems, we propose a magnetically guided catheter tipped with a solenoid rather than onboard magnetic materials. Although catheters with coils have been investigated under magnetic resonance imaging

Received 5 May 2024; accepted 11 September 2024. Date of publication 27 September 2024; date of current version 10 October 2024. This article was recommended for publication by Associate Editor S. Zuo and Editor P. Valdastrri upon evaluation of the reviewers' comments. This work was supported in part by the City University of Hong Kong under Project 7020061, and in part by the Research Grants Council of the Hong Kong Special Administrative Region, China, under Projects CityU 21202822 and CityU 11212321. (Corresponding authors: Jiachen Zhang; Jun Liu; Kiwon Ban.)

Xinliang Wang and Jiachen Zhang are with the Department of Biomedical Engineering, City University of Hong Kong, Hong Kong SAR, China (e-mail: xlwang.bme@my.cityu.edu.hk; jzhang.bme@cityu.edu.hk).

Weida Kang and Xudong Liang are with the School of Science, Harbin Institute of Technology, Shenzhen 518172, China (e-mail: kangweida@stu.hit.edu.cn; liangxudong@hit.edu.cn).

Kiwon Ban is with the Department of Biomedical Sciences, City University of Hong Kong, Hong Kong SAR, China (e-mail: ban.kw@cityu.edu.hk).

Jun Liu is with the Department of Data and Systems Engineering, The University of Hong Kong, Hong Kong SAR, China (e-mail: djliu@hku.hk).

This letter has supplementary downloadable material available at <https://doi.org/10.1109/LRA.2024.3469818>, provided by the authors.

Digital Object Identifier 10.1109/LRA.2024.3469818

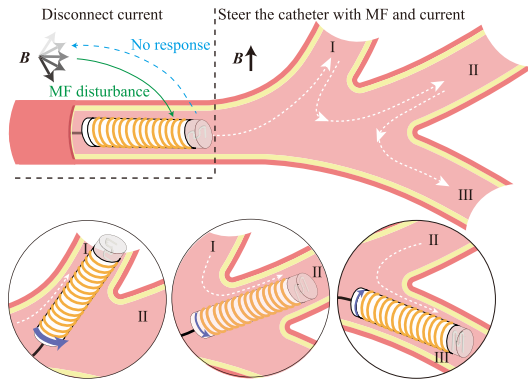


Fig. 1. Conceptual schematic showing the catheter tipped with a solenoid navigating inside a bifurcated vein. Upon disconnecting the current, the catheter is inactivated and unresponsive to the external MF's disturbance. During the navigation with the available MF, the catheter steers to the branch I by running a strong current. Reducing the current strength results in a small bending angle for alignment with the entrance of branch II without reorienting B . As for branch III, the catheter bends inversely via reversing the current's direction. Currents running through the solenoid in all branches are indicated by blue arrows. The white dashed lines present the catheter's motion trajectory.

before [20], [21], there is little discussion on the maneuverability safety and benefits brought by a solenoid or the feasibility of using an external permanent magnet or the electromagnetic coil to guide the catheter integrated with a coil. The controllable magnitude and direction of the magnetic moment introduced by the solenoid could eliminate or reduce the potential risks associated with permanent magnetic materials in attraction mode. It also facilitates the catheter to pass through bifurcations with multiple branches flexibly, as shown in Fig. 1. Most concerned thermal safety is experimentally evaluated under water. Reduced risk in attraction mode is verified by inputting frequency-controlled current. Subsequently, the catheter's bending capability is optimized and characterized in 3D space. Both static calibration and dynamic response tests are conducted to examine the soft force sensor's force-sensing ability. In experiments, we demonstrate the catheter's navigating functionality inside a 2D bifurcation model and an aortic arch 3D phantom. To further exhibit its potential employment in clinics, the magnetic catheter is advanced into a heart chamber phantom for demonstrating lesion navigation, force exertion, and tip trajectory control capabilities. The results suggest that our proposed catheter shows promise to become an efficient tool for conducting cardiac interventional therapy such as RFA in the future.

II. DESIGN AND FABRICATION

This section presents the design and fabrication process of the proposed magnetically driven catheter, tipped with a solenoid for remote steering and a soft force sensor for detecting the contact force.

A. Design of the Magnetically Guided Catheter

The proposed catheter utilizes a solenoid as its tip to enable magnetic navigation. Compared with previous studies using permanent magnetic materials [7], [13], both the direction and magnitude of the magnetic moment produced by the solenoid are

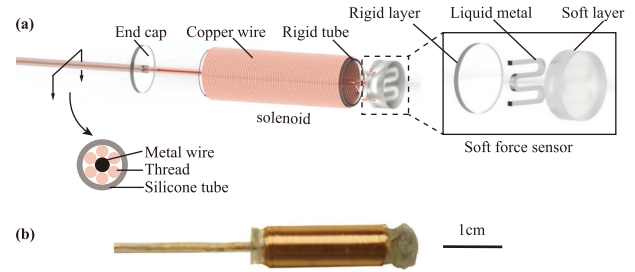


Fig. 2. Structural components and the prototype of the magnetically guided catheter. (a) The explosive view shows the catheter's constitution, which contains an end cap, a solenoid composed of a rigid tube and a wrapped copper wire, and a soft force sensor. The metal wire for delivering the catheter and six threads are packed inside a silicone tube, shown in a cross-section view. A detailed view exhibits the layered components of the soft force sensor. (b) A prototype of the magnetic catheter.

TABLE I
SIZES OF THE CATHETER'S COMPONENTS

Component	Diameter	Thickness	Length
Copper wire	0.20 mm	-	-
Thermal protection layer	-	0.20 mm	-
Soft force sensor	6.60 mm	3.40 mm	-
Microfluidic channel	0.33 mm	-	-
NiTi wire	0.25 mm	-	-
Solenoid	7.20 mm	-	23 mm

conveniently adjustable via input currents. Equation (1) gives a simplified model to demonstrate this theoretically [22].

$$\mathbf{m} = n\mathbf{I}A, \quad (1)$$

where n represents the loop number of the solenoid, \mathbf{I} is the input current, A indicates the solenoid's cross-section area, and \mathbf{m} represents the magnetic moment generated by the solenoid. The magnitude of \mathbf{m} is proportional to the amplitude of the input current \mathbf{I} . The direction of the magnetic moment \mathbf{m} is purely defined by that of the input current \mathbf{I} . Thus, the magnitude of the magnetic moment induced by the solenoid becomes controllable and consecutively adjustable. By reversing the current's direction, the magnetic moment instantly reorients its direction correspondingly. This property brings an additional method to control the catheter with the absence of maneuvering MF, which is particularly useful when the workspace for the MF source is limited.

The proposed catheter comprises a hyperelastic metal wire and a solenoidal tip integrated with a soft force sensor. In Fig. 2(a), a hollow hard tube plays the role of the catheter tip's backbone. The copper wire is wound around the surface of the hard tube to form a solenoid. At the distal end of the tube, a disk-shaped soft force sensor is installed to monitor the contact force between the catheter's tip and its surroundings. The soft force sensor is composed of a soft layer, a liquid metal layer, and a rigid layer. The soft layer is carved with a serpentine groove inward, where the liquid metal later fills in to create a flexible electrical circuit. Once the normal force is applied on the surface, the resulting deformation varies the liquid metal's electrical resistance, capturing and transforming the normal force into

measurable electrical resistance variation. The soft layer and rigid layer are tightly sealed together to prevent leakage of the liquid metal. Dual threads for each electrode of the soft force sensor are introduced for precise sensing. A hyperelastic metal wire is connected to the solenoid by passing through an end cap for advancing and retrieving the catheter. All threads and the metal wire are embraced by a silicone tube for compactness and thermal protection.

B. Fabrication of the Magnetically Guided Catheter

This catheter had multiple isolated components fabricated by different means. A copper wire was wrapped up to 273 loops in a unidirectional way and bonded to an acrylic tube by the cyanoacrylate adhesive (JL498, JULI, China). Two ends of the copper wire passed through the pinholes on the acrylic tube's side wall. Thereby the wire was held inside the acrylic tube for compactness. A mixture of components A and B (Ecoflex 00-10, Smooth-On, USA) with a mass ratio of 1:1 was coated on the coil as the thermal protection layer.

The soft force sensor was fabricated by employing a combination of 3D printing and mold-casting. Firstly, a miniaturized disk container and a cap were designed as the casting mold. An M-shaped convex line on the cap's interior surface is used to fabricate microfluidic channels on the soft layer. A 3D printer (3Pro Plus, Raise3D, USA) made this set of molds using polylactic acid. Next, silicone components A and B (Ecoflex 00-50, Smooth-On, USA) were mixed with a mass ratio of 1:1 at room temperature and pressure. After degassing in a vacuum chamber at 0.14 MPa for 5 minutes, the liquid silicone was cast into the mold for solidification. Next, the solidified silicone layer was peeled off from the mold. The silicone's surface carved with the M-shaped microchannel was bonded with a comparable-sized acrylic disk to seal the microchannel using flexible silicone glue (5562-B, KAIBINGTUAN, China). A syringe injected the Eutectic Gallium-Indium (EGaIn, HUATAI, China) into the microchannel. Four copper wires were inserted into the two inlets of the microchannel and fixed by flexible silicone glue. Lastly, the soft sensor was installed at the distal tip of the catheter using cyanoacrylate adhesive. A circular acrylic end cap with a central pinhole was glued at the bottom of the acrylic tube. A nickel-titanium (NiTi) wire and all threads passed through the end cap and were enveloped by a polyethylene tube. Table I lists the sizes of the magnetically actuated catheter's components.

III. CHARACTERIZATION

This section describes multiple examinations on the catheter's performance, including thermal safety, steerability, and force sensing capability. Firstly, temperature detection is carried out under various input currents to check the possibility of thermal damage to tissues. Subsequently, the effects of the actuating distance and the catheter's own gravity, which are considered important factors that can impact the catheter's bending performance, are explored thoroughly. Proceeding from the calibration between the force and the electrical resistance, the dynamic response of the soft force sensor is tested under input signals with various frequencies.

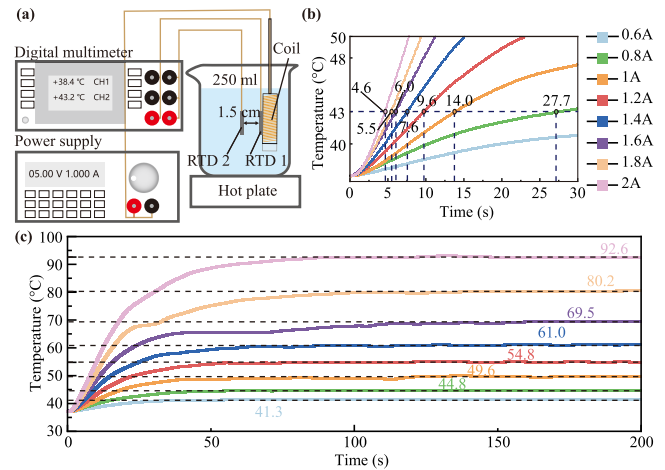


Fig. 3. Monitoring the temperature of the working solenoid and measuring thermally safe operation period (TSOP) to ensure thermal safety in catheterization. (a) Experimental setup for sensing the surface temperature of the solenoid underwater. (b) Required time for currents ranging from 0.6 to 2 A to heat up to thermal safety threshold. (c) The complete temperature curve for the 200 s heating process, including the steady-state temperature related to various input currents. Refer legend in (b).

A. Characterization of the Temperature Rise in Operation

In situations where the magnetic flux density is insufficient to bend the catheter adequately, increasing the current in the tipped solenoid could produce significant deflection, guiding the catheter to the desired position. Nevertheless, high currents produce massive Joule heat and raise the temperature of the solenoid. To strike a balance between better steering performance and thermal safety, the temperature variation of the solenoid tip was recorded underwater for estimation and analysis. In Fig. 3(a), two resistance temperature detectors (RTD, Heraeus RTD100, Germany) were connected to a digital multimeter (DMM6500, Keithely, USA) for data acquisition. The RTD 1 was attached to the solenoid's surface while the RTD 2 was placed in water, keeping a small distance of 1.5cm away from the former to detect the environment temperature. The water of 250 ml at room temperature, aiming to simulate the fluidic environment inside the vein, was initially prepared to immerse the magnetic catheter's tip. A hot plate compensated for water heat dissipation to maintain 37 °C, using feedback from RTD 2.

The temperature trends over the initial 30 seconds are shown in Fig. 3(b), illustrating the time required for the temperature to reach the thermal safety threshold with current ranging from 0.6 to 2 A. The steady-state temperature in a continuous 200 s detection is shown in Fig. 3(c). The raised temperature induced by the input current of 0.6 A is always no more than the safety threshold of 43 °C [23]. As for other input currents, the final temperatures were all beyond the safety threshold, meaning continuously operating the catheter carrying currents of these values is gravely detrimental to the human body. However, it does not mean that the intensity of current greater than 0.6 A is prohibited, since the maximum temperature of the solenoid is partially determined by the current conducting period.

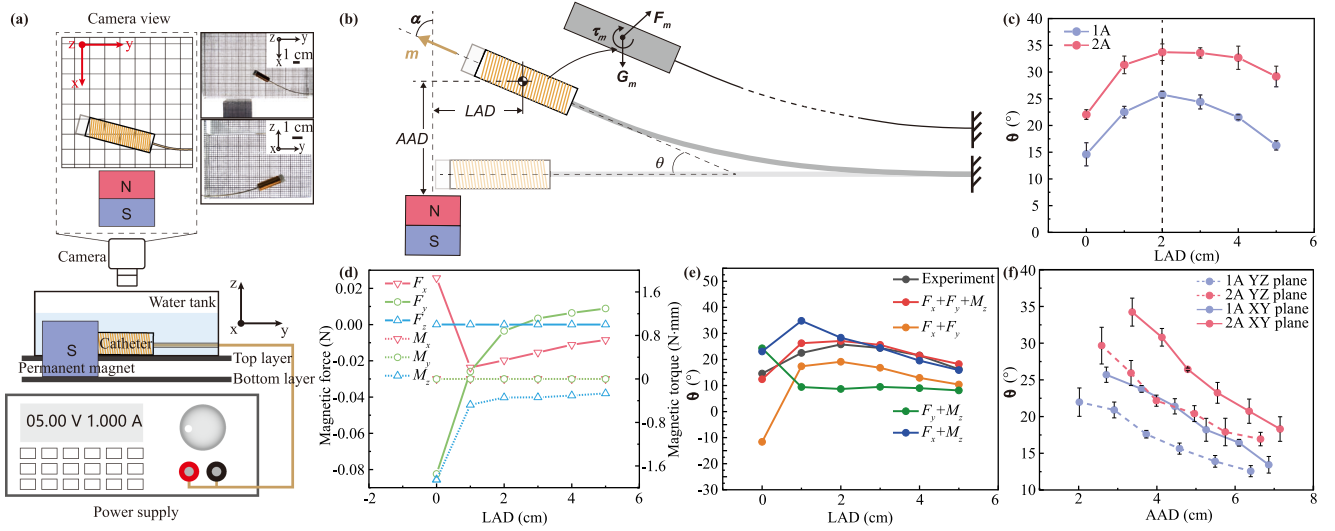


Fig. 4. Steerability optimization and characterization. (a) Experiment setup for characterizing the bending performance of the catheter. (b) Schematic illustration on magnetic deflection parameters and a mechanical model for the catheter's deflection. The bending angle θ is formed between the axial axis of the catheter's tip and the horizontal line. Horizontal and vertical separations between the centroid of the cubic permanent magnet's front face and the mass center of the catheter's tip are defined as LAD and AAD, respectively. (c) Variation of the bending angle θ over LAD. (d) The magnetic force and torque applied to the catheter's tip during scanning LAD. (e) The bending angles experimentally measured and ones theoretically calculated under different load combinations with an input current of 1 A on the XY plane. (f) The bending angle varies over AAD with input currents of 1 A and 2 A on the XY plane and the YZ plane. (error bar: 3σ with 5 trials. σ : standard deviation).

To further demonstrate the feasibility of applying huge currents in the aspect of thermal safety, we defined the thermally safe operation period (TSOP), beginning with turning on the current and ending with that surface temperature reaches up to 43°C . TSOP experimentally measured under a variety of input currents had been marked in Fig. 3(b). Fitting measured discrete TSOP data based on the heat transfer model generated a function, $y = 2.56/(0.196x - 0.0284)$ with $R^2 = 0.972$. It could theoretically predict TSOP relating to currents that were not tested in experiments.

B. Characterization of the Catheter's Steerability

In tortuous lumens, the catheter actively deflects the distal tip toward the targeted direction, causing less contact with surroundings and helping itself travel smoothly and efficiently. Here, we focus on the catheter's bending performance and explore the impact brought by lateral actuating distance (LAD), axial actuating distance (AAD), and current intensity on the catheter's deflection in 3D space. The experimental layout is depicted in Fig. 4(a).

A non-magnetic platform with top and bottom load layers held a water tank and two 38 mm side-length cubic NdFeB magnets (BX8X8X8-N52, K&J Magnetics, USA) in series, respectively. The catheter was connected to an adjustable direct current power source. On the top layer, the catheter was placed in the water tank and submerged in water. A piece of coordinate paper was attached to the bottom surface of the tank to facilitate the measurement. The steerability was intuitively quantified by the bending angle θ in Fig. 4(b). The mass center of the catheter's tip was maintained on the middle plane of permanent magnets. All bending tests were conducted in repulsive mode [24], with available magnetic flux intensity ranging from 15.60 to 352.60 mT.

With this experimental setup, we explored the effect that LAD has on bending angle, which had never been investigated before. LAD was scanned on the XY plane accompanied by a constant AAD of 3 cm. In Fig. 4(c), regardless of the input currents, the bending angle rises as LAD increases from 0 to 2 cm with an interval of 1 cm and finally reaches the maximum. Subsequently, it declines slowly as LAD increases from 2 to 5 cm. To figure out this phenomenon, a finite element model was established in COMSOL (COMSOL Multiphysics 5.6, Stockholm, Sweden) to quantitatively analyze the variation of magnetic torque τ_m and force F_m during the LAD scanning process in Fig. 4(d). The magnetic force and torque [6] applied to the catheter's tip during the LAD scanning were calculated by (2) and (3).

$$\tau_m = \mathbf{m} \times \mathbf{B} = \begin{bmatrix} 0 & I_y & -I_z \\ -I_x & 0 & I_z \\ I_x & -I_y & 0 \end{bmatrix} \begin{bmatrix} B_x \\ B_y \\ B_z \end{bmatrix} \quad (2)$$

$$\mathbf{F}_m = (\mathbf{m} \cdot \nabla) \mathbf{B} = nA \left(\begin{bmatrix} I_x \\ I_y \\ I_z \end{bmatrix} \cdot \begin{bmatrix} \frac{d}{dx} \\ \frac{d}{dy} \\ \frac{d}{dz} \end{bmatrix} \right) \begin{bmatrix} B_x \\ B_y \\ B_z \end{bmatrix} \quad (3)$$

Here \mathbf{m} is the magnetic moment generated by the energized solenoid and \mathbf{B} is the magnetic flux density at the solenoid. τ_m and F_m represent the magnetic torque and force applied to the catheter's tip, respectively.

Referring to the actuation profile on the XY plane in Fig. 4(a), negative τ_z and negative F_x contribute to the upward bending motion, while negative F_y straightens the catheter and decreases the bending angle θ . For LAD in the range of 0 to 2 cm, the blocking magnetic forces, negative F_y and positive F_x , decrease continuously while the negative M_z is falling at this stage. When LAD ranges from 2 to 5 cm, τ_z keeps almost a constant negative value, and negative F_x decreases gradually a little. Only positive

F_y has a little growth. Obviously, magnetic forces F_y and F_x are dominant factors responsible for the existence of optimized LAD.

To further demonstrate the effect each sole load has on the optimized LAD, magnetic torque τ_z , forces F_x and F_y derived from COMSOL were distributed into four load groups, which were exerted on the catheter's tip one by one using Abaqus (Abaqus 6.14, Dassault Systemes, French). Here gravity G_m was omitted on the XY plane. A superelastic model was adopted to analysis the catheter's deflection. Simulated results are shown in Fig. 4(e). Once all magnetic torque and force loads are applied to the catheter's tip, the simulated bending angle matches very well with that experimentally measured. Specifically, the peak of the bending angle only exists in load groups containing F_x . The load group with magnetic forces F_x and F_y generates a magnitude-reduced bending angle, but maintains the optimized LAD corresponding to the peak θ in the experiment. The load group with magnetic forces F_x and torque τ_z shifts the optimized LAD, however, holds the magnitude of the bending angle. By contrast, the magnetic force F_x and F_y determine the optimized LAD together.

Given the optimized LAD, the bending performance on the XY plane and the YZ plane is presented in Fig. 4(f) with input currents of 1 A and 2 A. The bending angle is negatively correlative to the AAD, regardless of the working planes or input currents. On the XY plane, as AAD approaches 3.6 and 2.7cm, the catheter could bend up to 35° and 25° with input currents of 2 A and 1 A, respectively. On the YZ plane, when AAD comes to 2.6 and 2.0 cm, the catheter steers up to 30° and 22° with input currents of 2 A and 1 A, respectively. It means that the steering capability of the catheter is controllable via input current and AAD. Moreover, bending performance measured on the XY plane and the YZ plane implies the catheter's steerability inside 3D space.

C. Characterization of the Catheter's Force-Sensing Capability

A soft force sensor based on the piezoresistance effect was designed to sense normal forces. The sensor's calibration and dynamic testing were conducted in the measurement platform (see Fig. 5(a)). A commercial force sensor (FSH04101, Fuek, USA) was employed to generate the reference force reading. The catheter's tip was constrained inside a 3D-printed fixture, with the soft force sensor centrally aligned with the load plate of the commercial force sensor. Both the catheter's tip and the commercial force sensor were installed on a lead screw linear guide. By manually rotating the lead screw during the calibration, the normal force could be tuned precisely with a minimum increment of 0.1 N. An Arduino microcontroller (UNO R3, Arduino, Italy) sent commands to a stepper motor, which drove the slider to move back and forth at a designated frequency for the dynamic test.

The calibration curve in Fig. 5(b) displays a positive correlation between the resistance variation ΔR and the normal force F_N . A linear fitting model, $\Delta R = 10.342 F_N$ was calculated with $R^2 = 0.99$ to map the normal force into the variation of

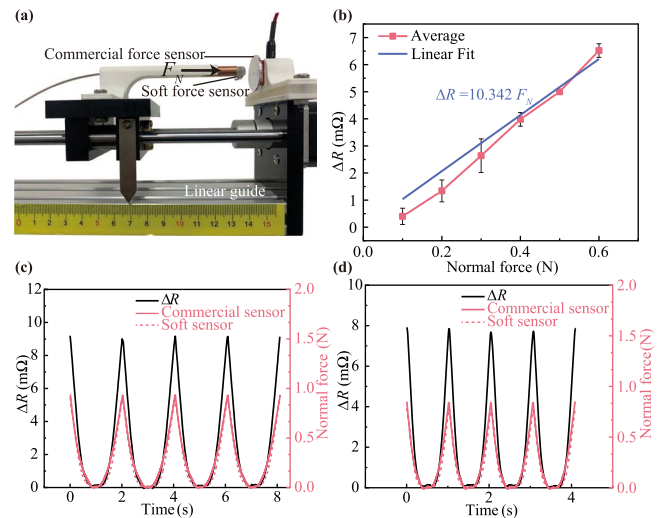


Fig. 5. Characterization on the soft force sensor. (a) Test setup for soft force sensor calibration and dynamic response. (error bar: 3σ with 5 trials) (b) The measured electrical resistance variation induced by the static normal force ranging from 0.1 to 0.6 N with an interval of 0.1 N and the calibration result based on a linear fitting. (c) Dynamic response curve under the normal force of 0.5 Hz and (d) 1 Hz.

electrical resistance. In dynamic tests, the fitting model was adopted to acquire force readings sensed by the soft force sensor. The dynamic response from the soft force sensor with the input frequency of 0.5 Hz and 1 Hz were shown in Fig. 5(c) and (d), respectively. The calibrated force had a good agreement with the reference force, proving the dynamic response of this soft force sensor reached up to 1 Hz.

IV. EXPERIMENT

In this section, the operation safety of the catheter in attraction mode was experimentally illustrated. Then the catheter was navigated inside a bifurcated channel and an aortic arch phantom to demonstrate the capability of remote steering, as well as the benefits brought by the solenoid tip. To mimic the RFA procedures, we delivered the catheter to reach specific markers distributed on the interior wall of a heart chamber phantom and applied specific forces. Furthermore, controlled tip trajectories in curve, straight line and circular path were displayed in the MF produced by Helmholtz coils.

A. Demonstration of Operation Safety

A magnetic catheter could achieve considerable deflection in attraction mode by manipulating it closer to the magnetic poles. However, larger deflection also further decreases the gap between the external magnet and the catheter. Once the actuating distance reduces to a critical value, where the stiffness could not counteract the huge magnetic force and torque for equilibrium, such a positive feedback control may cause the magnetic catheter to go out of control and crush into the lumen walls. We demonstrated this phenomenon in Fig. 6(a), in which the catheter was constantly input 1A current, working similar to that integrated with onboard magnetic materials, and positioned

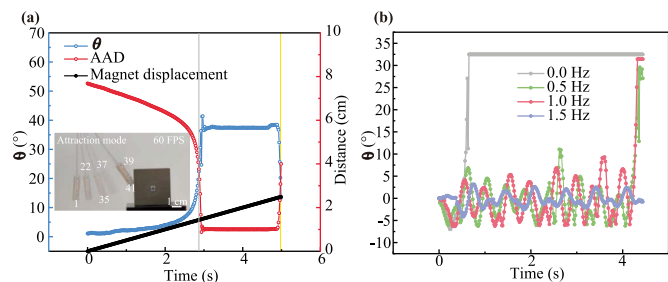


Fig. 6. Operation safety in attraction mode. (a) Conducting constant current, the catheter tipped with a coil works as a catheter consisting of onboard magnetic materials, which is easy to crush into the magnet in attraction mode after the magnet moves to a critical position (grey line). Disconnecting the current releases the catheter from the magnet (yellow line). (b) Comparison on the bending angle's variation corresponding to constant current and frequency controlled current in attraction mode.

at AAD of 7.4 cm and LAD of 0. Upon the permanent magnet arrived at a critical position (grey line), the bending angle θ rapidly increased while the AAD dropped quickly. Then the catheter's tip crushed to the magnet and was captured tightly. Only disconnecting the current (yellow line) could release it from the magnet.

Due to the adjustable magnetic moment based on current control, currents of various frequencies ranging from 0 to 1.5 Hz were tested in attraction mode to clarify the operation safety. As Fig. 6(b) shows, the magnetic catheter could be controlled for bending up to around 10° with frequency of 0.5 and 1 Hz and duty of 0.3 for 4 s without capture by the magnet. While for 1.5 Hz, bending angle seems too small to be utilized for navigation, but operation safety is ensured since no capture happens. For constant current (0 Hz), the catheter was instantly caught within 0.7 s. Although the catheter operated with 0.5 and 1 Hz current was ultimately captured, it could be released on time thanks to the disconnecting phase during the actuation period. Comparing with the onboard permanent magnetic materials, dragging away the external magnet is the only solution to detach the catheter, during which excessive contact force induced by the dragging motion leads to secondary injury.

B. Demonstrations of Magnetically Guided Navigation

A 2D bifurcated channel made up of 3D-printed parts and acrylic plates had a main channel and two branches with an intersection angle of 60° . The cross-section area of the bifurcation model kept a constant size of $13 \text{ mm} \times 8 \text{ mm}$. The catheter and bifurcation channel were immersed in water at 24°C in the experiment. A 38 mm side-length cubic permanent magnet was placed beside the bifurcation channel for actuation. Three groups of navigation demonstration with an input current of 1 A were executed on the XY plane and the YZ plane, as shown in Fig. 7(a).

In the demonstrations, we observed that the catheter was predictably blocked or randomly entered into one of the branches using manual advancement. Once the current was turned on and the current's direction was set as expected, the catheter headed to the targeted branch and could be smoothly fed forward. All navigating demonstrations were completed within 14 s (TSOP

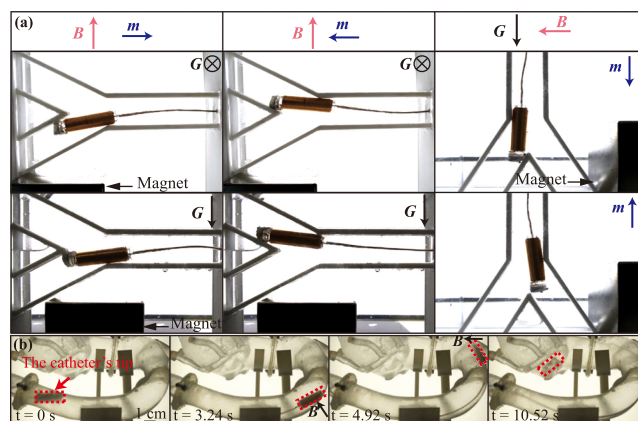


Fig. 7. Magnetically guided navigation in a bifurcated channel and an aortic arch phantom. (a) The catheter was magnetically navigated through a planar bifurcated channel in 3D space. (b) The catheter passed through an aortic arch phantom and ultimately entered the heart chamber with the assistance of external magnetic steering.

of 1 A). After withdrawal from the targeted branch, the catheter could bend oppositely via reversing the current, with no need for reorienting the external MF on the XY plane or the YZ plane. It is a convenient and safe approach compared with reconfiguring the external MF, particularly adopting a robotic arm to manipulate a permanent magnet, which wastes time on replanning the task path and exhibits limited mobility in narrow space.

To further explore the effectiveness of navigation in anatomic lumens, the catheter was transmitted into an aortic arch phantom in Fig. 7(b). The catheter marched into the descending aorta at a constant speed until the arch of aorta, which buckled the catheter and impeded the advancement. Once powering a current of 1 A, we manually operated two magnets (202020N52, Taobao, China) with 2 cm side-length in series for actuation. The catheter's tip was bent towards the center line of the artery, reducing the friction between the catheter's tip and the interior wall for advancement. The permanent magnets guided the electromagnetic tip along the aortic arch until the catheter entered the heart chamber. The whole navigating procedure finished within 11 s, which was considered as thermally safe. Navigation procedures inside the bifurcated channel and the aortic arch phantom were recorded in supplementary movies S1 and S2, respectively.

C. Demonstration of Cardiac Catheter Positioning and Trajectory Manipulation

The soft force sensor-tipped catheter is designed to navigate to targeted lesion sites and provide feedback on the force exerted on tissues. A real-sized, hollow, and semitransparent heart chamber phantom was adopted in experimental procedures, as shown in Fig. 8(a). Three markers were labeled on the exterior surface of the phantom. To begin with, the catheter had been navigated into the heart chamber filled with water. A 38 mm side-length cubic permanent magnet was held beside the catheter to produce a repulsive magnetic force and torque upon switching on the current and guide the solenoid tip to the designated position.

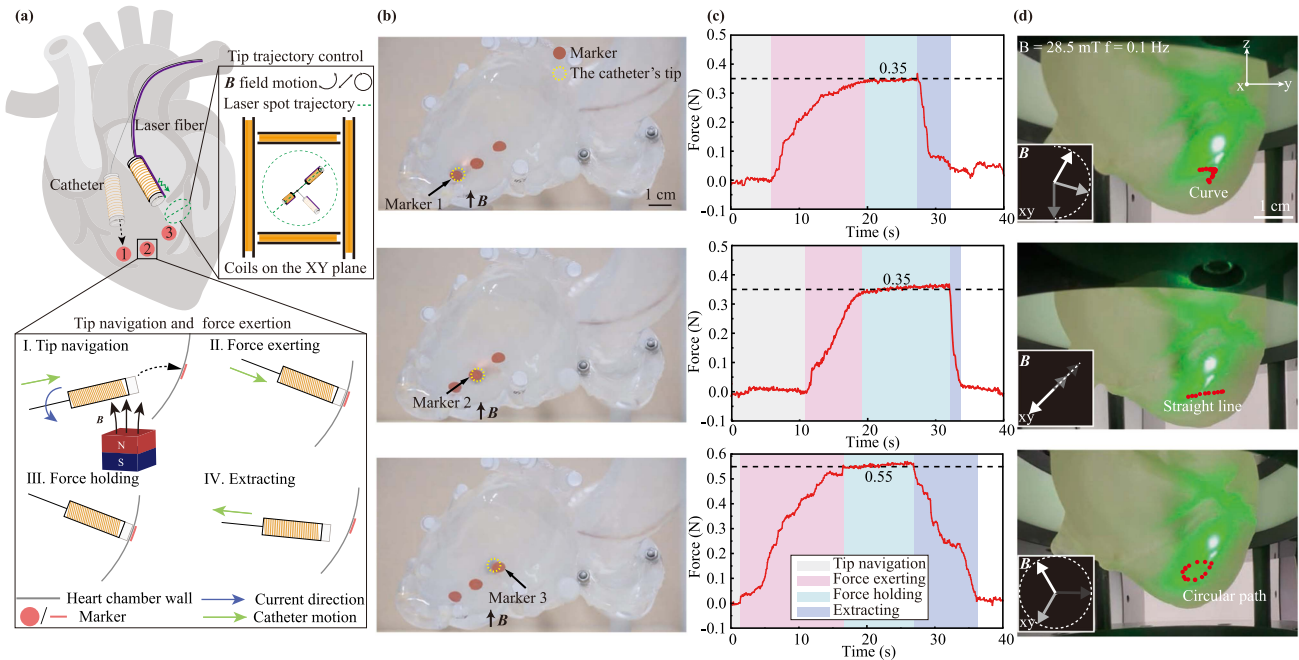


Fig. 8. Navigating the catheter's tip, exerting specific force and controlling the tip trajectory on the interior wall of a heart chamber phantom. (a) Schematic illustration of the tip navigation and force exerting experiment with permanent magnet, as well as tip trajectory control inside Helmholtz coils. The bottom enlarged figure exhibits four procedures: tip navigating, force exerting, force holding, and catheter extracting, to steer the catheter's tip to a particular marker and exert desired and constant force. The top right enlarged figure describes magnetic field motion and the predetermined laser spot trajectory. (b) The catheter's tip (yellow dash circle) was guided at the marker 1, the marker 2, and the marker 3 in sequence by controlling the external permanent magnet and input current. (c) Force curves recorded at three markers. (d) The trajectory of the laser spot produced by controlling the magnetic field on the XY plane inside the Helmholtz coils.

Once the catheter's tip reached the targeted marker, we fed the catheter a small distance to stabilize the contact between the interior wall of the phantom and the catheter's tip. Then we pushed the catheter gently and continuously to apply force. Once the feedback force met the expected one, the catheter was held on to keep a constant force for a specific period. Finally, we retrieved the catheter from the current marker and transferred it to the next position.

For markers 1 and 2 at relatively low sites, a current of 1 A was able to deflect the catheter toward the destination. For the marker 3 located at the highest position, only a current of 2 A could counteract the tip's own gravity and then lever it up toward the targeted site. Fig. 8(b) and (c) show successful tip navigation and force exerting, respectively. The soft force sensor recorded applied force data in Fig. 8(c). The plateaus appearing in force curves proved that we successfully applied a normal force of 0.35 N on markers 1 and 2, and 0.55 N on the marker 3. The tip navigation and force exerting process were available in supplementary movie S3.

Integration with laser fibers expands the catheter's application toward RFA. In Fig. 8(a), an optical fiber core attached with the catheter's tip, which emitted the green laser, was fed inside the heart chamber phantom. Both the catheter and the phantom located at a three-dimension Helmholtz coil's center. The uniform magnetic field was set with magnetic flux intensity of 28.5 mT and frequency of 0.1 Hz on the XY plane. The magnetic flux intensity B moved in three forms: semi-circular, reciprocating, and circular. With input current of 1 A, the laser spot's trajectories were shown in Fig. 8(d). The tip trajectories

were displayed in curves, straight lines, and circular paths. This achieves the stable ablation paths in RFA procedures, assisting surgeons in performing operations more confidently in confined spaces. The tip trajectory control is recorded in supplementary movie S4.

V. DISCUSSIONS AND CONCLUSIONS

Here, we designed and fabricated a magnetically actuated catheter tipped with a soft force sensor, working under the guidance of external permanent magnets and Helmholtz coils toward interventional treatment. To ensure its thermal safety in operation, temperature monitoring was conducted with the current's strength ranging from 0.6 to 2 A. As the catheter worked underwater, a current of 0.6 A could be the best choice when guiding along a long path since it contributed no thermal damage in a long period. In the situation where the catheter encountered sharp corners and required a current larger than 0.6 A, the fitted TSOP offered operators a referenced and conservative catheter operation period to protect human tissue against overheating. In practice, the heat generated by the solenoid could be reduced further by flowing blood [25], which was not taken into account in the TSOP measurement.

Throughout bending tests on the XY plane, we found the LAD was a key parameter that influenced the catheter's steerability when actuated by permanent magnets, which had not been researched in previous studies. We further explored the mechanism behind the optimized LAD and pinpointed the dominant magnetic forces. Therefore, LAD loses the efficacy of

improving steering performance in a homogeneous MF due to the dependence of magnetic forces on the MF's nonuniformity. Based on optimized LAD, the catheter could bend up to 35° on the *XY* plane and 30° on the *YZ* plane with input currents of 2 A. Bending in 3D space, particularly against its own gravity on the *YZ* plane, indicated the catheter's outstanding navigating capability for intervention treatment. To summarize, the proposed catheter's bending deformation under a permanent magnet depends on multiple factors, including LAD, AAD, and input currents. This provides the operators with multiple methods to control the catheter's deflection and navigate to desirable sites.

Frequency control on the current achieves usable deflection on proposed catheter in attraction mode. Moreover, disconnecting phase in the period releases the catheter from the external magnet to avoid secondary injury. The variable magnetic moment brought by the coil reduces the risks of magnetic capture and enhances the operation safety. The navigation in a bifurcated channel validates that the catheter could pass through the branches flexibly by only controlling the current without manipulating external MF source.

The proposed catheter shows great potential in MIS such as RFA. Remote placement and precise pressing force of the heat generator are always expected in the RFA procedure to reduce the bleeding, the unnecessary ablation depth of treated tissues due to the excessive force, and also the operators' radiation-absorbed dose. Our proposed catheter is able to travel across the aortic arch model and enter the heart chamber phantom under the actuation of external MF. It could remotely navigate a soft force sensor to designated positions inside the heart chamber phantom and apply precise force with a resolution of 0.1 N. The tip trajectory control capability with precisely controlled magnetic field reduces the surgical manipulation difficulty and provides various ablation paths such as curves, straight lines, and circular paths. Thus it offers a novel and safe solution for RFA treatment.

Great challenges still exist toward clinical usage for our proposed magnetic catheter. The limitation of our proposed catheter focuses on the oversize and overheat. Potential solutions could be found by compressing the hollowing space of the coil and introducing the heat sink or isolation material to the magnetic catheter. Besides, we will attempt to make the skeleton of the catheter's tip with elastic materials to improve its bending capability by reducing its stiffness. Enhancing the available magnetic flux intensity, such as working inside the MRI, is a feasible route to expand the catheter's deflection. The impact of temperature on soft force sensors should be considered in the future to improve measurement accuracy over long periods. The repeatability of soft force sensors also needs to be enhanced by improving the electrode structure to reduce the impact of contact resistance, as well as using stable silicone materials in their fabrication.

REFERENCES

[1] M. Runciman, A. Darzi, and G. P. Mylonas, "Soft robotics in minimally invasive surgery," *Soft Robot.*, vol. 6, no. 4, pp. 423–443, Aug. 2019.

- [2] Y. Bo et al., "Advancements in materials, manufacturing, propulsion and localization: Propelling soft robotics for medical applications," *Front. Bioeng. Biotechnol.*, vol. 11, Jan. 2024, Art. no. 1327441.
- [3] H. Wang, Y. Mao, and J. Du, "Continuum robots and magnetic soft robots: From models to interdisciplinary challenges for medical applications," *Micromachines*, vol. 15, no. 3, Mar. 2024, Art. no. 313.
- [4] C. Yang et al., "Geometric constraint-based modeling and analysis of a novel continuum robot with shape memory alloy initiated variable stiffness," *Int. J. Robot. Res.*, vol. 39, no. 14, pp. 1620–1634, 2020.
- [5] H. Bai et al., "Unlocking the potential of cable-driven continuum robots: A comprehensive review and future directions," *Actuators*, vol. 13, no. 2, Feb. 2024, Art. no. 52.
- [6] J. J. Abbott, E. Diller, and A. J. Petruska, "Magnetic methods in robotics," *Annu. Rev. Control, Robot., Auton. Syst.*, vol. 3, no. 1, pp. 57–90, 2020.
- [7] J. Lussi et al., "A submillimeter continuous variable stiffness catheter for compliance control," *Adv. Sci.*, vol. 8, no. 18, 2021, Art. no. 2101290.
- [8] M. Richter, V. K. Venkiteswaran, and S. Misra, "Concentric tube-inspired magnetic reconfiguration of variable stiffness catheters for needle guidance," *IEEE Robot. Automat. Lett.*, vol. 8, no. 10, pp. 6555–6562, Oct. 2023.
- [9] D. Lin, J. Wang, N. Jiao, Z. Wang, and L. Liu, "A flexible magnetically controlled continuum robot steering in the enlarged effective workspace with constraints for retrograde intrarenal surgery," *Adv. Intell. Syst.*, vol. 3, no. 10, 2021, Art. no. 2000211.
- [10] S. Jeon et al., "A magnetically controlled soft microrobot steering a guidewire in a three-dimensional phantom vascular network," *Soft Robot.*, vol. 6, no. 1, pp. 54–68, 2019.
- [11] S. Fu et al., "A magnetically controlled guidewire robot system with steering and propulsion capabilities for vascular interventional surgery," *Adv. Intell. Syst.*, vol. 5, no. 11, 2023, Art. no. 2300267.
- [12] Y. Cao et al., "Magnetic continuum robot with intraoperative magnetic moment programming," *Soft Robot.*, vol. 10, no. 6, pp. 1209–1223, Jul. 2023.
- [13] Y. Kim, G. A. Parada, S. Liu, and X. Zhao, "Ferromagnetic soft continuum robots," *Sci. Robot.*, vol. 4, no. 33, Aug. 2019, Art. no. eaax7329.
- [14] G. Pittiglio et al., "Patient-specific magnetic catheters for atraumatic autonomous endoscopy," *Soft Robot.*, vol. 9, no. 6, pp. 1120–1133, Dec. 2022.
- [15] P. Lloyd, O. Onaizah, G. Pittiglio, D. K. Vithanage, J. H. Chandler, and P. Valdastrì, "Magnetic soft continuum robots with braided reinforcement," *IEEE Robot. Automat. Lett.*, vol. 7, no. 4, pp. 9770–9777, Oct. 2022.
- [16] Q. Peng et al., "Thermal and magnetic dual-responsive catheter-assisted shape memory microrobots for multistage vascular embolization," *Research*, vol. 7, 2024, Art. no. 0339.
- [17] H. Wang et al., "Data-driven parallel adaptive control for magnetic helical microrobots with derivative structure in uncertain environments," *IEEE Trans. Syst., Man, Cybern.: Syst.*, vol. 54, no. 7, pp. 4139–4150, Jul. 2024.
- [18] S. Zhong et al., "Spatial constraint-based navigation and emergency re-planning adaptive control for magnetic helical microrobots in dynamic environments," *IEEE Trans. Autom. Sci. Eng.*, early access, Dec. 20, 2023, doi: 10.1109/TASE.2023.3339637.
- [19] C. Limpabandhu, Y. Hu, H. Ren, W. Song, and Z. T. Ho Tse, "Magnetically steerable catheters: State of the art review," *Proc. Inst. Mech. Engineers. Part H., J. Eng. Med.*, vol. 237, no. 3, pp. 297–308, Mar. 2023.
- [20] N. Gudino, J. A. Heilman, J. J. Derakhshan, J. L. Sunshine, J. L. Duerk, and M. A. Griswold, "Control of intravascular catheters using an array of active steering coils," *Med. Phys.*, vol. 38, no. 7, pp. 4215–4224, 2011.
- [21] L. Muller, M. Saeed, M. W. Wilson, and S. W. Hetts, "Remote control catheter navigation: Options for guidance under MRI," *J. Cardiovasc. Magn. Reson.*, vol. 14, no. 1, Jun. 2012, Art. no. 43.
- [22] F. Settecase et al., "Magnetically-assisted remote control (MARC) steering of endovascular catheters for interventional MRI: A model for deflection and design implications," *Med. Phys.*, vol. 34, no. 8, pp. 3135–3142, 2007.
- [23] P. S. Yarmolenko et al., "Thresholds for thermal damage to normal tissues: An upyear," *Int. J. Hyperthermia*, vol. 27, no. 4, pp. 320–343, 2011.
- [24] Y. Kim et al., "Telerobotic neurovascular interventions with magnetic manipulation," *Sci. Robot.*, vol. 7, no. 65, 2022, Art. no. eabg9907.
- [25] T. Roberts, W. Hassenzahl, S. Hetts, and R. Arenson, "Remote control of catheter tip deflection: An opportunity for interventional MRI," *Magn. Reson. Med.*, vol. 48, no. 6, pp. 1091–1095, 2002.